Design and Simulation of a Guidance Control System for a 2.75-inch Rocket Using Pole Placement and PI Control

Nathawat Chaikam[1], Prasatporn Wongkamchang[2*] and Prayoon Kunyoo[3]

[1,3]Graduate School, Navaminda Kasatriyadhiraj Royal Air Force Academy

[2]Department of Mechanical Engineering, Navaminda Kasatriyadhiraj Royal Air Force Academy

prasatporn_w@rtaf.mi.th

Received 03 March 2025

Revised 27 May 2025

Accepted 17 August 2025

Abstract

This research focuses on the design and simulation of an autopilot system for a 2.75-inch Wrap-Around Fin Aerial Rocket (WAFAR), incorporating a guidance system into the traditional unguided airframe. The control system was designed using a combination of pole placement techniques and proportional-integral (PI) control to enable precise directional control and maintain stability during flight. The design process takes into account the dynamics and aerodynamic characteristics of the rocket. The pole placement technique was employed to define the pole locations in the system's transfer function, achieving the desired stability and response characteristics. Concurrently, the PI control enhances the system's responsiveness and tracking accuracy. The guidance of the rocket is achieved through acceleration control, enabling it to follow the desired trajectory. A nonlinear simulation of the rocket under different launch-to-target distances and LOS errors demonstrates the effectiveness and accuracy of the proposed control system in target tracking. Although the control system was designed based on a linearized model of the rocket dynamics, it was evaluated on a nonlinear plant model to verify its practical performance.

Keywords: Guidance Control, Pole Placement, PI Control, 2.75-inch Rocket

1. Introduction

Continuous advancement of military weapon capabilities is essential. The 2.75-inch rocket is a widely used military weapon due to its ease of installation and straightforward operation. However, its accuracy in actual operations heavily relies on the pilot’s skill, and errors can occur when engaging moving targets. This limitation arises because the rocket lacks the ability to adjust its trajectory once launched. Therefore, integrating a guidance system into the rocket's structure is a necessary development to enhance its operational effectiveness.

The conventional 2.75-inch rocket is designed without a control system and relies on high-speed spin stabilization to maintain flight stability. This characteristic makes the design of an in-flight trajectory control system particularly challenging and complex. The control system design must account for nonlinear dynamics, the rocket's unique aerodynamic properties, and external disturbances that may affect performance.

Previous studies have explored guidance system enhancements for the 2.75-inch rocket. For instance, the U.S. Army's Advanced Precision Kill Weapon System (APKWS) utilizes canard fin adjustments to modify the rocket's direction mid-flight [1]. The Skid-to-Turn autopilot system for APKWS has been designed and simulated to evaluate its performance [2]. Additionally, alternative guidance systems, such as the Hit-to-Kill Rocket Guidance Kit (Model HKGK), have been developed and analyzed, utilizing reaction thrusters for directional control [3]. These studies demonstrate the ongoing research and development of guidance systems for the 2.75-inch rocket.

While many existing approaches employ advanced control techniques such as model predictive control (MPC) or adaptive control, these methods often require high computational resources and complex implementation. In contrast, the method proposed in this study offers a practical trade-off between simplicity and performance robustness. This research focuses on designing a control system that prioritizes target-tracking accuracy while maintaining rocket stability under various flight conditions. A hybrid control approach is proposed, integrating Pole Placement and PI control. The Pole Placement technique is employed to modify the rocket's dynamic response by appropriately positioning the system's transfer function poles, ensuring both stability and desired performance. Meanwhile, PI control is incorporated to enhance system responsiveness and maintain accurate trajectory tracking. The guidance law follows a Proportional Navigation (PN) strategy to determine the required acceleration, followed by the designed control system, which determines the magnitude of the reaction thrust. Furthermore, the maximum angle of attack is constrained to preserve flight stability.

The proposed control system is evaluated through nonlinear simulations using a 6-degree-of-freedom (6-DOF) model implemented within the CADAC++ framework [4], a high-fidelity simulation tool for missile guidance and flight dynamics. This simulation provides a comprehensive assessment of the developed control system's performance and effectiveness.

2. Methods

This section presents the equations governing the rocket's motion dynamics and their transformation into a linearized form. The equations are then reformulated into the state-space representation. The next step involves designing the directional control system.

Due to the limitations of the Model HKGK guidance design, which prevents roll plane control, the control system is designed to regulate pitch and yaw motions using reaction thrust located within the guidance section. After presenting the relevant mathematical equations, the subsequent section will focus on simulation and performance analysis.

2.1 Nonlinear Equations of Motion

To accurately study the control of the rocket's motion and perform an in-depth analysis, the 6-DOF equations of motion are utilized (Fig. 1).

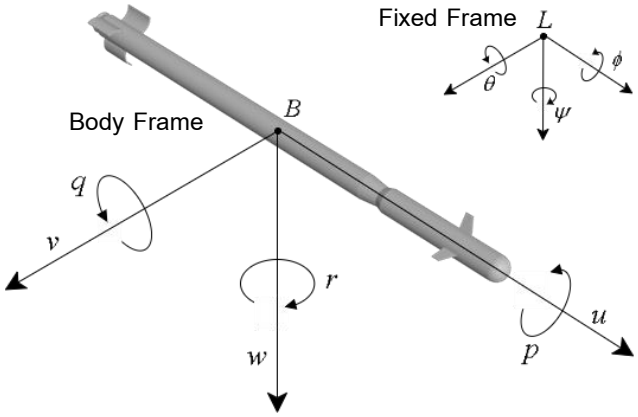

Fig 1 The 6-DOF equation of motion in the body frame

The translational equations of motion are derived based on Newton's second law.

$$\left[\frac{d\left(mV_B^E\right)}{dt}\right]^E = F + mG$$

And from the Transport Theorem.

$$\left[\frac{dV_B^E}{dt}\right]^E = \left[\frac{dV_B^E}{dt}\right]^B + \left[\Omega^{BE}\right]^B \left[V_B^E\right]^B$$

This leads to the translational equations of motion, which are presented in Equation (1).

$$m\left[\frac{dV_B^E}{dt}\right]^B + m\left[\Omega^{BE}\right]^B \left[V_B^E\right]^B = \left[F\right]^B + m\left[T\right]^{BL}\left[G\right]^L \tag{1}$$

The formulation of the rotational equations of motion begins with Euler's equations of rotational dynamics.

$$\left[\frac{d\left(I_B^B\omega^{BE}\right)}{dt}\right]^E = M_B$$

By applying the Transport Theorem and assuming a constant moment of inertia for the rocket, the rotational equations of motion can be derived as shown in Equation (2).

$$\left[I_B^B\right]^B\left[\frac{d\omega^{BE}}{dt}\right]^B + \left[\Omega^{BE}\right]^B\left[I_B^B\right]^B\left[\omega^{BE}\right]^B = \left[M_B\right]^B \tag{2}$$

where: $\left[V_B^E\right]^B = \begin{bmatrix} u & v & w \end{bmatrix}^T$, $\left[\omega^{BE}\right]^B = \begin{bmatrix} p & q & r \end{bmatrix}^T$,

$$\left[\Omega^{BE}\right]^B = \begin{bmatrix} 0 & -r & q \\ r & 0 & -p \\ -q & p & 0 \end{bmatrix}, \quad \left[I_B^B\right]^B = \begin{bmatrix} I_{11} & 0 & 0 \\ 0 & I_{22} & 0 \\ 0 & 0 & I_{22} \end{bmatrix}$$

The symbols used in Equations (1) and (2) are defined as follows: m is the mass of the rocket [kg]; V_B^E is the velocity vector of the rocket with respect to(wrt) the earth frame [m/s]; Ω^{BE} is the angular velocity vector of the rocket frame wrt the earth frame in the form of a skew-symmetric matrix [rad/s]; $[T]^{BL}$ is the transformation matrix to convert values from the flat Earth coordinate system to the rocket body coordinate system; G is the gravitational force vector [N]; I_B^B is the Moment of Inertia (MOI) tensor of the rocket referred to the rocket's center of gravity (c.g.) [kg·m^2]; ω^{BE} is the angular velocity vector of the rocket frame wrt the earth frame [rad/s]; F is the force vector, consisting of the Thrust vector (F_t), Reaction Thrust vector (F_{rt}), and Aerodynamic Force vector (F_a) [N]; M_B is the moment vector, consisting of moments generated by the Reaction Thrust (M_{rt}) and Aerodynamic Moment (M_a) [N·m]; $[*]^B$ and $[*]^L$ are the vector or tensor * expressed in the body and the local-level coordinate system, respectively.

Equations (1) and (2) describe the motion of the rocket, including both translational motion and rotational motion along the Roll, Pitch, and Yaw axes. These equations are nonlinear differential equations, where the nonlinearities arise from terms such as the product of velocity and angular velocity in Equation (1), and the cross product of angular velocity and angular momentum in Equation (2).

The terms of Aerodynamic Force and Moment can be expressed in terms of Aerodynamic Coefficients, as shown in Fig. 2.

$$\left[F_a\right]^B = \bar{q}S\begin{bmatrix} -C_A & C_Y & -C_N \end{bmatrix}^T$$
$$\left[M_a\right]^B = \bar{q}Sd\begin{bmatrix} C_l & C_m & C_n \end{bmatrix}^T$$

where $\bar{q}$ is the dynamic pressure [N/m^2]; S is the reference area [m^2]; d is the rocket diameter [m]; C_A, C_Y, C_N, C_l, C_m and C_n are the axial force coefficient, side force coefficient, normal force coefficient, rolling moment coefficient, pitching moment coefficient, and yawing moment coefficient, respectively.

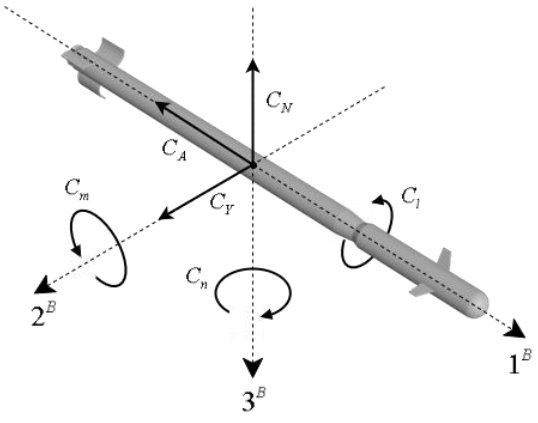

Fig 2 Force and moment aerodynamics coefficient

2.2 Linearization and State Space Equation

The control system used for the direction control of the rocket in this research utilizes a PI controller combined with pole placement techniques, which is a classical control method. This approach is suitable for linear systems. However, since the motion equations (1) and (2) describe a nonlinear system, a direct design of the control system is not possible. Therefore, linearization must be performed prior to design. It is assumed that changes in the rocket's direction are considered a small perturbation to the system. Under this assumption, the state of the system can be expressed as the sum of a reference component and a perturbation component. That is,

$$\mathrm{x}_p = R^{BpBr}\mathrm{x}_r + \varepsilon\mathrm{x}$$

where x_p and x_r are the state vectors at the perturbed and reference flights, respectively; $\varepsilon\mathrm{x}$ is the perturbation; R^{BpBr} is the rotation tensor of the perturbed frame wrt the reference frame.

By substituting each variable in Equation (1) with the summation of its reference and perturbation components, the following expression is obtained:

$$m\left[\frac{d\left(R^{BpBr}V_{Br}^{E}+\varepsilon V_{B}^{E}\right)}{dt}\right]^{Bp}+m\left[\left(R^{BpBr}\Omega^{BrE}\overline{R^{BpBr}}+\varepsilon\Omega^{BE}\right)\right]^{Bp}\left[\left(R^{BpBr}V_{Br}^{E}+\varepsilon V_{B}^{E}\right)\right]^{Bp}$$
$$=\left[\left(R^{BpBr}F_r+\varepsilon F\right)\right]^{Bp}+m\left[\left(R^{BpBr}G_r+\varepsilon G\right)\right]^{Bp}$$

where ω^{BpBr} is the angular velocity vector of the perturbed rocket frame wrt the reference rocket frame [rad/s]; $[*]^{Bp}$ and $[*]^{Br}$ are the vector or tensor * expressed in the perturbed and the reference coordinate system, respectively.

In the present analysis, a steady reference flight condition is assumed, in which the reference flight is considered non-accelerated and non-rotating.

$$m\left[\frac{d\left(R^{BpBr}\right)}{dt}\right]^{Bp}\left[V_{Br}^{E}\right]^{Bp}+\underline{m\left[R^{BpBr}\right]^{Bp}\left[\frac{d\left(V_{Br}^{E}\right)}{dt}\right]^{Bp}}+m\left[\frac{d\left(\varepsilon V_{B}^{E}\right)}{dt}\right]^{Bp}$$
$$\underline{+m\left[\varepsilon\Omega^{BE}\right]^{Bp}\left[R^{BpBr}\right]^{Bp}\left[V_{Br}^{E}\right]^{Bp}}+m\left[\varepsilon\Omega^{BE}\right]^{Bp}\left[\varepsilon V_{B}^{E}\right]^{Bp}$$
$$=\underline{\left[R^{BpBr}\right]^{Bp}\left[F_r\right]^{Bp}}+\left[\varepsilon F\right]^{Bp}+\underline{m\left[R^{BpBr}\right]^{Bp}\left[G_r\right]^{Bp}}+m\left[\varepsilon G\right]^{Bp}$$

The underlined term corresponds to the translational motion of the reference flight, rotated by a rotation tensor. Since the rotation tensor appears identically on both sides of the equation, the term cancels out. Together with the relations defined as:

$$\varepsilon\Omega^{BE}=\Omega^{BpE}-R^{BpBr}\Omega^{BrE}\overline{R^{BpBr}}$$
$$\omega^{BpE}=\omega^{BpBr}+\omega^{BrE}$$

Based on the above assumptions, the equation can be reformulated as:

$$m\left[\frac{d\left(R^{BpBr}\right)}{dt}\right]^{Bp}\left[V_{Br}^{E}\right]^{Bp}+m\left[\frac{d\left(\varepsilon V_{B}^{E}\right)}{dt}\right]^{Bp}+m\left[\Omega^{BpBr}\right]^{Bp}\left[\varepsilon V_{B}^{E}\right]^{Bp}=\left[\varepsilon F\right]^{Bp}+m\left[\varepsilon G\right]^{Bp}$$

Under the assumption of small perturbation, the relation can be approximated as:

$$\frac{d\left(R^{BpBr}\right)}{dt} \approx \Omega^{BpBr} R^{BpBr}$$

Together with the relation $\left[\overline{R^{BpBr}}\right]^{Bp} = [T]^{BpBr}$, it follows that

$$m\left[\Omega^{BpBr}\right]^{Bp}\left[V_{Br}^{E}\right]^{Br} + m\left[\frac{d\left(\varepsilon V_B^E\right)}{dt}\right]^{Bp} + \underline{m\left[\Omega^{BpBr}\right]^{Bp}\left[\varepsilon V_B^E\right]^{Bp}} = [\varepsilon F]^{Bp} + m[\varepsilon G]^{Bp}$$

The underlined term remains nonlinear of second order. In the context of small perturbation analysis, this term becomes negligibly small and can therefore be omitted. Furthermore, to simplify the control system design, the term $m\left[\Omega^{BpBr}\right]^{Bp}\left[V_{Br}^{E}\right]^{Br}$, as well as the gravity force and thrust force terms, are also excluded from consideration.

The forces and moments generated by aerodynamics typically depend on multiple variables, which are nonlinear functions.

$$\begin{aligned}\varepsilon F_a = F_{ap} - F_{ar} = {} & \frac{\partial F_a}{\partial V_B^E}\left(\varepsilon V_B^E\right) + \frac{1}{2!}\frac{\partial^2 F_a}{\partial V_B^{E2}}\left(\varepsilon V_B^E\right)^2 + \frac{1}{3!}\frac{\partial^3 F_a}{\partial V_B^{E3}}\left(\varepsilon V_B^E\right)^3 + \ldots \\ & + \frac{\partial F_a}{\partial \omega^{BpBr}}\left(\omega^{BpBr}\right) + \frac{1}{2!}\frac{\partial^2 F_a}{\partial \omega^{BpBr2}}\left(\omega^{BpBr}\right)^2 + \frac{1}{3!}\frac{\partial^3 F_a}{\partial \omega^{BpBr3}}\left(\omega^{BpBr}\right)^3 + \ldots \\ & + \frac{\partial F_a}{\partial \dot{V}_B^E}\left(\varepsilon \dot{V}_B^E\right) + \frac{1}{2!}\frac{\partial^2 F_a}{\partial \dot{V}_B^{E2}}\left(\varepsilon \dot{V}_B^E\right)^2 + \frac{1}{3!}\frac{\partial^3 F_a}{\partial \dot{V}_B^{E3}}\left(\varepsilon \dot{V}_B^E\right)^3 + \ldots\end{aligned}$$

By considering small variations and using a Taylor series expansion, the nonlinear functions can be approximated to linear forms by discarding the higher-order terms. The linearized equation of motion can then be written as follows.

$$m\left[\frac{d\varepsilon V_B^E}{dt}\right]^{Bp} = \left[\frac{\partial F_a}{\partial V_B^E}\right]^{Bp}\left[\varepsilon V_B^E\right]^{Bp} + \left[\frac{\partial F_a}{\partial \omega^{BpBr}}\right]^{Bp}\left[\omega^{BpBr}\right]^{Bp} + \left[\frac{\partial F_a}{\partial \dot{V}_B^E}\right]^{Bp}\left[\varepsilon \dot{V}_B^E\right]^{Bp} + [\varepsilon F_{rt}]^{Bp} \quad (3)$$

Given the definitions $[F_a]^{Bp} = \begin{bmatrix} X & Y & Z \end{bmatrix}^T$ and $[F_{rt}]^{Bp} = \begin{bmatrix} 0 & T_y & -T_z \end{bmatrix}^T$, the decomposition of the matrix components can be expressed as:

$$m\begin{bmatrix}\dot{u}\\ \dot{v}\\ \dot{w}\end{bmatrix} = \begin{bmatrix}\frac{\partial X}{\partial u} & \frac{\partial X}{\partial v} & \frac{\partial X}{\partial w}\\ \frac{\partial Y}{\partial u} & \frac{\partial Y}{\partial v} & \frac{\partial Y}{\partial w}\\ \frac{\partial Z}{\partial u} & \frac{\partial Z}{\partial v} & \frac{\partial Z}{\partial w}\end{bmatrix}\begin{bmatrix}u\\ v\\ w\end{bmatrix} + \begin{bmatrix}\frac{\partial X}{\partial p} & \frac{\partial X}{\partial q} & \frac{\partial X}{\partial r}\\ \frac{\partial Y}{\partial p} & \frac{\partial Y}{\partial q} & \frac{\partial Y}{\partial r}\\ \frac{\partial Z}{\partial p} & \frac{\partial Z}{\partial q} & \frac{\partial Z}{\partial r}\end{bmatrix}\begin{bmatrix}p\\ q\\ r\end{bmatrix} + \begin{bmatrix}\frac{\partial X}{\partial \dot{u}} & \frac{\partial X}{\partial \dot{v}} & \frac{\partial X}{\partial \dot{w}}\\ \frac{\partial Y}{\partial \dot{u}} & \frac{\partial Y}{\partial \dot{v}} & \frac{\partial Y}{\partial \dot{w}}\\ \frac{\partial Z}{\partial \dot{u}} & \frac{\partial Z}{\partial \dot{v}} & \frac{\partial Z}{\partial \dot{w}}\end{bmatrix}\begin{bmatrix}\dot{u}\\ \dot{v}\\ \dot{w}\end{bmatrix} + \begin{bmatrix}0\\ T_y\\ -T_z\end{bmatrix}$$

In this context, X , Y and Z represent the first, second, and third components of the aerodynamic force vector, respectively. These components can be expressed as $X = -A$, where A is the axial force, Y is the side force, and $Z = -N$, where N is the normal force. T_y and T_z are the side force and normal force from the reaction thrust, respectively [N].

For the rotational equations of motion, a similar linearization approach can be applied under the small perturbation assumption, as was done for the translational case.

By defining $[M_a]^{Bp} = \begin{bmatrix} LL & M & LN \end{bmatrix}^T$ and $[M_{rt}]^{Bp} = \begin{bmatrix} 0 & T_z\left(x_{cg} - x_t\right) & T_y\left(x_{cg} - x_t\right) \end{bmatrix}^T$, the linearized rotational equations of motion can be written as:

$$\left[I_{Bp}^{Bp}\right]^{Bp}\left[\frac{d\omega^{BpBr}}{dt}\right]^{Bp}=\left[\frac{\partial M_a}{\partial V_B^E}\right]^{Bp}\left[\varepsilon V_B^E\right]^{Bp}+\left[\frac{\partial M_a}{\partial \omega^{BpBr}}\right]^{Bp}\left[\omega^{BpBr}\right]^{Bp}+\left[\frac{\partial M_a}{\partial \dot{V}_B^E}\right]^{Bp}\left[\varepsilon \dot{V}_B^E\right]^{Bp}+\left[\varepsilon M_{rt}\right]^{Bp} \tag{4}$$

$$\begin{bmatrix} I_{11} & 0 & 0 \\ 0 & I_{22} & 0 \\ 0 & 0 & I_{22} \end{bmatrix}\begin{bmatrix} \dot{p} \\ \dot{q} \\ \dot{r} \end{bmatrix}=\begin{bmatrix} \frac{\partial LL}{\partial u} & \frac{\partial LL}{\partial v} & \frac{\partial LL}{\partial w} \\ \frac{\partial M}{\partial u} & \frac{\partial M}{\partial v} & \frac{\partial M}{\partial w} \\ \frac{\partial LN}{\partial u} & \frac{\partial LN}{\partial v} & \frac{\partial LN}{\partial w} \end{bmatrix}\begin{bmatrix} u \\ v \\ w \end{bmatrix}+\begin{bmatrix} \frac{\partial LL}{\partial p} & \frac{\partial LL}{\partial q} & \frac{\partial LL}{\partial r} \\ \frac{\partial M}{\partial p} & \frac{\partial M}{\partial q} & \frac{\partial M}{\partial r} \\ \frac{\partial LN}{\partial p} & \frac{\partial LN}{\partial q} & \frac{\partial LN}{\partial r} \end{bmatrix}\begin{bmatrix} p \\ q \\ r \end{bmatrix}$$

$$+\begin{bmatrix} \frac{\partial LL}{\partial \dot{u}} & \frac{\partial LL}{\partial \dot{v}} & \frac{\partial LL}{\partial \dot{w}} \\ \frac{\partial M}{\partial \dot{u}} & \frac{\partial M}{\partial \dot{v}} & \frac{\partial M}{\partial \dot{w}} \\ \frac{\partial LN}{\partial \dot{u}} & \frac{\partial LN}{\partial \dot{v}} & \frac{\partial LN}{\partial \dot{w}} \end{bmatrix}\begin{bmatrix} \dot{u} \\ \dot{v} \\ \dot{w} \end{bmatrix}+\begin{bmatrix} 0 \\ T_z\left(x_{cg}-x_t\right) \\ T_y\left(x_{cg}-x_t\right) \end{bmatrix}$$

where LL, M and LN are the rolling moment, pitching moment, and yawing moment, respectively [N·m]; x_{cg} and x_t are the distances between the c.g. and the position of the reaction thrust from the rocket's nose, respectively [m].

From Equations (3) and (4), the complexity of the calculations can be reduced by minimizing the number of aerodynamic force and moment terms. This can be achieved by applying the derivative map [5], which selectively includes only the derivative terms that have a significant influence on the forces and the moments acting on the rocket. As a result, the equations can be reformulated in scalar form as follows:

$$\begin{aligned} m\dot{u} &= X_u u + X_{\dot{u}}\dot{u} \\ m\dot{v} &= Y_v v + Y_r r + Y_{\dot{v}}\dot{v} + T_y \\ m\dot{w} &= Z_w w + Z_q q + Z_{\dot{w}}\dot{w} - T_z \end{aligned} \tag{5}$$

$$\begin{aligned} I_{11}\dot{p} &= LL_p p \\ I_{22}\dot{q} &= M_w w + M_q q + M_{\dot{w}}\dot{w} + T_z\left(x_{cg}-x_t\right) \\ I_{22}\dot{r} &= LN_v v + LN_r r + LN_{\dot{v}}\dot{v} + T_y\left(x_{cg}-x_t\right) \end{aligned} \tag{6}$$

Since there is no control over the rotational motion in the roll plane, the equations related to the motion in the roll plane can be discarded. In terms of aerodynamic force and moment, the variables v, w, $\dot{v}$ and $\dot{w}$ can be replaced with the sideslip angle (β), angle of attack (α), side acceleration (a_l), and normal acceleration (a_n), respectively. By neglecting the less significant terms, Equations (5) and (6) can be rewritten as Equations (7) and (8), respectively.

$$\begin{aligned} ma_l &= Y_\beta \beta + T_y \\ ma_n &= -Z_\alpha \alpha + T_z \end{aligned} \tag{7}$$

$$\begin{aligned} I_{22}\dot{q} &= M_\alpha \alpha + M_q q + T_z\left(x_{cg}-x_t\right) \\ I_{22}\dot{r} &= LN_\beta \beta + LN_r r + T_y\left(x_{cg}-x_t\right) \end{aligned} \tag{8}$$

When considering small perturbation in the angle of attack, the relationship between normal acceleration and the flight path angle (γ) can be expressed by Equation (9).

$$a_n = V\dot{\gamma} \tag{9}$$

Similarly, the relationship between side acceleration and the heading angle (χ) is given by Equation (10).

$$a_l = V\dot{\chi} \tag{10}$$

$$\dot{\gamma} = q - \dot{\alpha} \text{ and } \dot{\chi} = r + \dot{\beta}$$

where V is the relative speed [m/s].

By taking the derivative of Equation (7) and substituting the values from Equations (9) and (10), and neglecting the dynamics of the reaction thrusters, the equations can be rewritten as Equations (11) and (12).

$$\begin{aligned} m\dot{a}_l &= \frac{Y_\beta}{V} a_l - Y_\beta r \\ m\dot{a}_n &= \frac{Z_\alpha}{V} a_n - Z_\alpha q \end{aligned} \tag{11}$$

$$\begin{aligned} I_{22}\dot{q} &= -\frac{mM_\alpha}{Z_\alpha} a_n + M_q q + T_z\left(x_{cg} - x_t\right) \\ I_{22}\dot{r} &= \frac{mLN_\beta}{Y_\beta} a_l + LN_r r + T_y\left(x_{cg} - x_t\right) \end{aligned} \tag{12}$$

where $Y_\beta = \bar{q}SC_{Y_\beta}$; $Z_\alpha = -\bar{q}SC_{N_\alpha}$; $M_\alpha = \bar{q}SdC_{m_\alpha}$;

$M_q = \frac{\bar{q}Sd^2}{2V} C_{m_q}$; $LN_\beta = \bar{q}SdC_{n_\beta}$ and $LN_r = \frac{\bar{q}Sd^2}{2V} C_{n_r}$

From Equations (11) and (12), a state-space equation for a linear system can be formulated in the following form.

$$\dot{\mathrm{x}} = \mathrm{Ax} + \mathrm{Bu}$$

$$\mathrm{y} = \mathrm{Cx}$$

This can be divided into two motion directions: the longitudinal equation and the lateral equation.

$$\mathrm{x}_{long} = \begin{bmatrix} q & a_n \end{bmatrix}^T$$

$$\mathrm{x}_{lat} = \begin{bmatrix} r & a_l \end{bmatrix}^T$$

$$\mathrm{u}_{long} = T_z$$

$$\mathrm{u}_{lat} = T_y$$

$$\mathrm{A}_{long} = \begin{bmatrix} \frac{M_q}{I_{22}} & 0 \\ -\frac{Z_\alpha}{m} & \frac{Z_\alpha}{mV} \end{bmatrix}, \ \mathrm{A}_{lat} = \begin{bmatrix} \frac{LN_r}{I_{22}} & 0 \\ -\frac{Y_\beta}{m} & \frac{Y_\beta}{mV} \end{bmatrix},$$

$$\mathrm{B}=\begin{bmatrix}\dfrac{(x_{cg}-x_t)}{I_{22}}\\ 0\end{bmatrix},\ \mathrm{C}=\begin{bmatrix}0 & 1\end{bmatrix}$$

Variables followed by the subscript "$long$" refer to the variables associated with the longitudinal direction, while "lat" refers to variables related to the lateral direction. Variables without a subscript are used for both longitudinal and lateral directions.

2.3 Autopilot Design for HKGK Model

A widely used method for controlling the direction of a missile to track a target is acceleration control, chosen due to its high accuracy. In this study, this method was chosen, and a hybrid control technique combining pole placement and a PI controller was employed. The control system can be represented by the block diagram shown in Fig. 3.

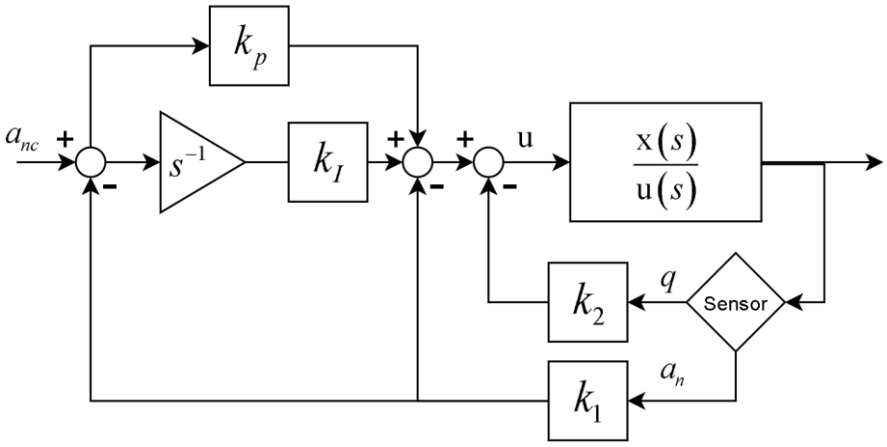

Fig 3 Normal acceleration control by pole placement technique and PI controller

From Fig. 3**,** the system can be separated into two feedback loops: The inner loop consists of the pole placement technique, which includes the acceleration loop and the rate loop. The rate loop is added to enhance the stability of the system. The outer loop consists of the PI controller, which is used to control the response speed and reduce steady-state errors in acceleration.

The transfer function of the system can be obtained by taking the Laplace transformation of the state space equation. The result will be.

$$s\mathrm{x}(s)=\mathrm{A}\mathrm{x}(s)+\mathrm{B}\mathrm{u}(s)$$
$$\mathrm{y}(s)=\mathrm{C}\mathrm{x}(s)$$

where $\mathrm{u}(s)=\begin{bmatrix}-k_2 & -k_p-\dfrac{k_I}{s}-k_1\end{bmatrix}\begin{bmatrix}q(s)\\ a_n(s)\end{bmatrix}+\left(k_p+\dfrac{k_I}{s}\right)a_{nc}(s)$, which can be written as $\mathrm{u}(s)=\mathrm{a}_1\mathrm{x}(s)+\mathrm{a}_2\mathrm{u}'(s)$

By substituting the value of $\mathrm{u}(s)$ into the state space equation and rearranging, the new equation will be.

$$\begin{aligned} s\mathrm{x}(s) &= \mathrm{A}\mathrm{x}(s) + \mathrm{B}\left[\mathrm{a}_1\mathrm{x}(s) + \mathrm{a}_2\mathrm{u}'(s)\right] \\ \left[s\mathrm{I} - \left(\mathrm{A} + \mathrm{B}\mathrm{a}_1\right)\right]\mathrm{x}(s) &= \mathrm{B}\mathrm{a}_2\mathrm{u}'(s) \\ \left[s\mathrm{I} - \mathrm{A}'\right]\mathrm{x}(s) &= \mathrm{B}'\mathrm{u}'(s) \end{aligned}$$

The poles of the system can be obtained from the eigenvalues of the matrix A' by considering the characteristic equation of the system.

$$\mathrm{Det}\left(s\mathrm{I} - \mathrm{A}'\right) = 0$$

When substituted with the matrix, the result will be.

$$\mathrm{Det}\left(\begin{bmatrix} s - \dfrac{M_q}{I_{22}} + \dfrac{(x_{cg} - x_t)k_2}{I_{22}} & \dfrac{(x_{cg} - x_t)\left(k_p + \dfrac{k_I}{s} + k_1\right)}{I_{22}} \\ \dfrac{Z_\alpha}{m} & s - \dfrac{Z_\alpha}{mV} \end{bmatrix}\right) = 0$$

This can then be written as the equation.

$$s^3 + \mathrm{a}_m s^2 + \mathrm{b}_m s + \mathrm{c}_m = 0 \tag{13}$$

where

$$\begin{aligned} \mathrm{a}_m &= -\left(\frac{M_q}{I_{22}} + \frac{Z_\alpha}{mV} - \frac{(x_{cg} - x_t)k_2}{I_{22}}\right) \\ \mathrm{b}_m &= -\left(\frac{(x_{cg} - x_t)Z_\alpha k_1}{mI_{22}} - \frac{M_q Z_\alpha}{mVI_{22}} + \frac{(x_{cg} - x_t)Z_\alpha k_p}{mI_{22}} + \frac{(x_{cg} - x_t)Z_\alpha k_2}{mVI_{22}}\right) \\ \mathrm{c}_m &= -\frac{(x_{cg} - x_t)Z_\alpha k_I}{mI_{22}} \end{aligned}$$

From the cubic polynomial equation, it can be rewritten in terms of the damping ratio (ζ) and natural frequency (ω_n) as shown in equation (14).

$$\begin{aligned} \left(s + p\right)\left(s^2 + 2\zeta\omega_n s + \omega_n^2\right) &= 0 \\ s^3 + \left(2\zeta\omega_n + p\right)s^2 + \left(\omega_n^2 + 2p\zeta\omega_n\right)s + p\omega_n^2 &= 0 \end{aligned} \tag{14}$$

where $\left(s + p\right)$ is the factor of the polynomial that gives a real pole, with the pole positioned at $-p$ on the s-plane.

By comparing equations (13) and (14), the following is obtained.

$$(2\zeta\omega_n + p) = -\left(\frac{M_q}{I_{22}} + \frac{Z_\alpha}{mV} - \frac{(x_{cg} - x_t)k_2}{I_{22}}\right)$$

$$(\omega_n^2 + 2p\zeta\omega_n) = -\left(\frac{(x_{cg} - x_t)Z_\alpha k_1}{mI_{22}} - \frac{M_q Z_\alpha}{mVI_{22}} + \frac{(x_{cg} - x_t)Z_\alpha k_p}{mI_{22}} + \frac{(x_{cg} - x_t)Z_\alpha k_2}{mVI_{22}}\right)$$

$$p\omega_n^2 = -\frac{(x_{cg} - x_t)Z_\alpha k_I}{mI_{22}}$$

And the gain value can be calculated as shown in Equation (15).

$$k_I = -\frac{mpI_{22}\omega_n^2}{(x_{cg} - x_t)Z_\alpha}$$

$$k_2 = \frac{I_{22}}{(x_{cg} - x_t)}\left(p + 2\omega_n\zeta + \frac{M_q}{I_{22}} + \frac{Z_\alpha}{mV}\right) \quad (15)$$

$$k_1 = -\frac{mI_{22}}{(x_{cg} - x_t)Z_\alpha}\left(\omega_n^2 + 2p\omega_n\zeta + \frac{2\omega_n\zeta Z_\alpha}{mV} + \frac{pZ_\alpha}{mV} + \frac{Z_\alpha^2}{m^2V^2}\right) - k_p$$

For lateral acceleration control, it can be done in the same way as for normal acceleration. Finally, the gain equation for lateral control is given in (16).

$$k_I = -\frac{mpI_{22}\omega_n^2}{(x_{cg} - x_t)Y_\beta}$$

$$k_2 = \frac{I_{22}}{(x_{cg} - x_t)}\left(p + 2\omega_n\zeta + \frac{LN_r}{I_{22}} + \frac{Y_\beta}{mV}\right) \quad (16)$$

$$k_1 = -\frac{mI_{22}}{(x_{cg} - x_t)Y_\beta}\left(\omega_n^2 + 2p\omega_n\zeta + \frac{2\omega_n\zeta Y_\beta}{mV} + \frac{pY_\beta}{mV} + \frac{Y_\beta^2}{m^2V^2}\right) - k_p$$

The gain k_1, k_2 and k_I will be recalculated continuously to keep the pole positions of the system at their appropriate locations as defined.

The design of the HKGK model's attitude control will be adjusted using the thrust forces from three reaction thrusters in the guidance system, with their positions arranged as shown in Fig. 4.

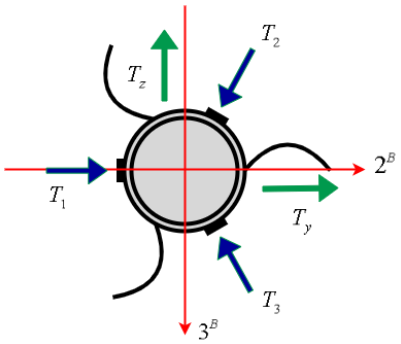

Fig 4 The positions and directions of the reaction thrust vectors

The thrust force generated by each reaction thruster is related to the resultant side force (T_y) and normal force (T_z) according to Equation (17).

$$T_y = T_1 - (T_2 + T_3)\sin\left(\frac{\pi}{6}\right)$$
$$T_z = (T_3 - T_2)\cos\left(\frac{\pi}{6}\right) \quad (17)$$

where T_1, T_2 and T_3 are the thrust forces from reaction thrusters at positions 1, 2, and 3, respectively [N].

3. Simulation and Evaluation

3.1 Simulation Using the CADAC++ Framework

The simulation framework Computer Aided Design of Aerospace Concepts (CADAC) was originally developed using FORTRAN and later upgraded to C++ for its advantages in object-oriented programming. This updated version is referred to as CADAC++ [4]. CADAC++ is a framework designed to assist in the development and simulation of complex dynamic systems, particularly in the context of aerospace, aviation, and autonomous control systems. It allows for accurate simulation of the motion and control of these systems. In addition, CADAC++ can simulate noise or disturbances from both sensors and environmental conditions, which further enhances the reliability of the simulations.

In this study, the direction control of a 2.75-inch aerial rocket is simulated using the CADAC++ framework. A 6-DOF model is used to provide the most realistic analysis possible. The rocket follows a semi-active guidance system, where it receives target position signals from a laser designated by ground forces. For the simulation, it is assumed that the rocket can detect the target's position via the laser sensor even before launch. Upon launch, after approximately 1.3 seconds, which is the time when thrust from the rocket's engine runs out, the rocket enters the terminal phase and starts using the designed control system for direction control. This simulation assumes that throughout the entire flight, the rocket can always detect the target's position.

From the 1.3-second mark onward, the rocket enters the terminal phase, accurately guiding toward the target. The control system begins calculating acceleration commands using the PN guidance law. The acceleration command is then sent to the control system to be converted into the required thrust values to adjust the rocket’s direction using reaction thrust. The control system continuously receives the rocket's status after each reaction thrust operation and makes adjustments accordingly, until the rocket either hits the target or impacts the ground. The overall working diagram is shown in Fig. 5.

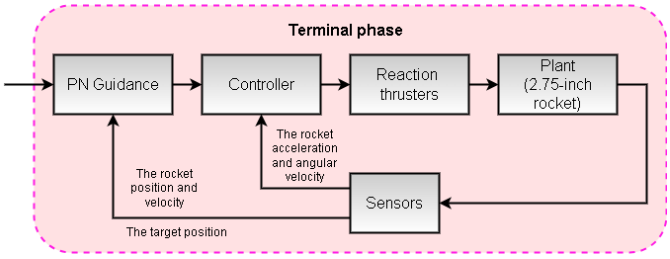

Fig 5 Overview of the rocket simulation operation

For the conditions of the simulation, it is assumed that the M151 warhead is used, which affects the various physical properties of the rocket. The distance between the rocket and the target is set from 4 to 9 km along the ground, with the target remaining stationary. The rocket's altitude at launch is 1 km above the ground level. The aircraft is assumed to fly at a speed of 185 m/s while launching the rocket. The LOS error, which includes Azimuth error ($\Delta\psi$) and Elevation error ($\Delta\theta$) at the moment of launch, is set between -30 to 30 degrees. These errors are related to the rocket's pitch and yaw angles as shown in equation (18).

$$\begin{aligned} \psi_0 &= \psi_{LOS} + \Delta\psi \\ \theta_0 &= \theta_{LOS} + \Delta\theta \end{aligned} \tag{18}$$

where ψ_0 and θ_0 are the Yaw and Pitch angles of the rocket at the moment of launch, respectively; ψ_{LOS} and θ_{LOS} are the Azimuth and Elevation angles of the LOS, respectively.

In the simulation, the effects of the changing mass and Moment of Inertia (MOI) of the rocket while flying are taken into account. Furthermore, limits are set for the acceleration command signals to ensure that the angle of attack and side slip do not exceed 20 degrees, which helps maintain the stability of the rocket during flight control.

3.2 Simulation Performance Evaluation

The performance analysis is divided into two main aspects: the response of the rocket's acceleration control system and the accuracy of the rocket. These analyses provide insights into the overall effectiveness of the rocket with an integrated guidance system. The details of each aspect are as follows:

3.2.1 Control System Response Analysis

The acceleration control system was designed using a hybrid approach combining pole placement and a PI controller, as described in Section 2.3. This design requires specifying the system's pole locations by defining the constants ζ , ω_n , and p , which influence both the system's stability and response characteristics. Additionally, the gain k_P can be adjusted to fine-tune the system's response sensitivity.

For a 2.75-inch rocket, a rapid response is essential because the rocket has a very short time to reach the target. Since directional control begins approximately 1.3 seconds after launch, a slow response could significantly reduce targeting accuracy. At the same time, maintaining stability during flight is crucial to ensure the reliability of the control system.

From the simulation, the constants were set to $\zeta = 0.7$, $\omega_n = 9.8$ rad/s, $p = 40$ rad/s and $k_P = 1$. The resulting normal acceleration response of the control system is shown in Fig. 6.

From the response shown in Fig. 6, the rocket's normal acceleration effectively follows the control system's command and reaches a steady-state value relatively quickly. This is because the natural frequency was set to a relatively high value. However, a slight overshoot occurs during the initial response to control signal changes due to the use of a damping ratio less than 1, which results in an underdamped system behavior.

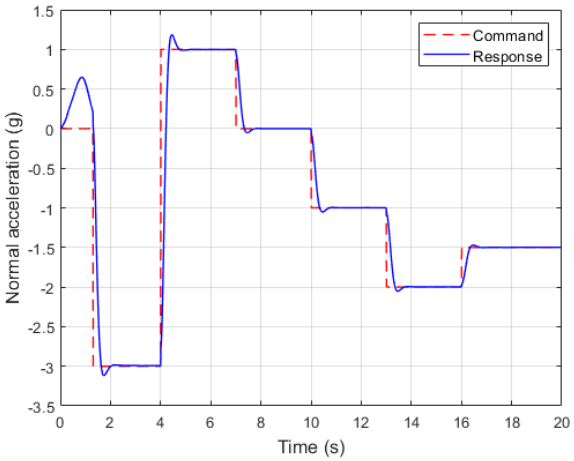

Fig 6 Normal acceleration response of the control system

When examining the steady-state normal acceleration, there is only minor oscillation in the signal. This oscillation is negligible and does not exhibit any tendency to grow over time, ensuring that the system remains stable. Therefore, the control system successfully provides a rapid response while maintaining stability throughout the flight.

To confirm that the rocket maintains stability while undergoing acceleration control, the angle of attack (AOA) during flight can be analyzed, as shown in Fig. 7. The angle varies in response to the acceleration command, exhibiting minor oscillations only during the initial phase of signal changes. These transient oscillations do not significantly affect the overall stability of the rocket.

Additionally, during the steady-state phase, where acceleration signals fluctuate slightly, these variations do not impact the stability of the angle of attack at that moment. This indicates that the control system effectively maintains stable flight characteristics throughout the maneuver.

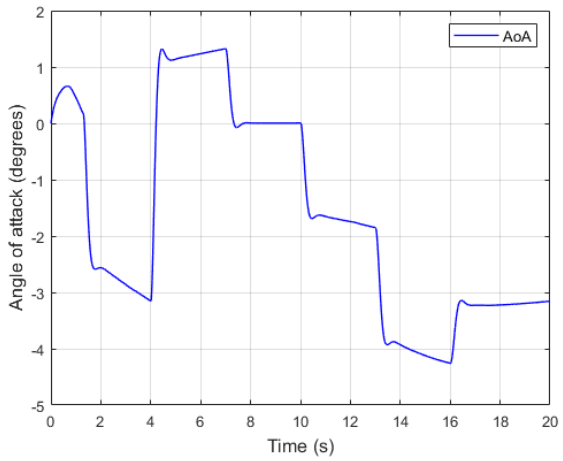

Fig 7 Angle of attack during normal acceleration control

The response of the lateral acceleration control signal exhibits a similar behavior to that of the normal acceleration when the same constant values are applied. The system maintains stability while effectively responding to control commands, ensuring precise maneuverability of the rocket.

3.2.2 Accuracy Analysis

The accuracy assessment is conducted through a simulated rocket launch under the conditions described in Section 3.1, assuming that each reaction thruster produces a maximum thrust of 4.9 N. Accuracy is evaluated based on the miss distance between the rocket and the target, using the c.g. as a reference point for both objects. The miss distance is measured when the rocket reaches the ground, ensuring that the c.g. positions of the rocket and the target are at the same altitude. The results of the simulated launches are presented in Tables 1–6.

Table 1: Miss Distance at a Rocket-to-Target Displacement of 4000 m

$\Delta\psi \setminus \Delta\theta$ (degrees)	-10	-5	0	5	10	15	20	25	30
-30	>50	>50	>50	>50	>50	>50	>50	>50	>50
-25	>50	>50	>50	>50	>50	>50	>50	>50	>50
-20	>50	>50	>50	>50	>50	>50	>50	>50	>50
-15	>50	>50	>50	>50	>50	>50	>50	>50	>50
-10	>50	>50	>50	26.7041	>50	>50	>50	>50	>50
-5	>50	>50	0.0902	0.0676	>50	>50	>50	>50	>50
0	>50	43.3668	0.0921	0.0696	23.2308	>50	>50	>50	>50
5	>50	>50	2.8069	18.6418	32.7264	>50	>50	>50	>50
10	>50	>50	>50	>50	>50	>50	>50	>50	>50
15	>50	>50	>50	>50	>50	>50	>50	>50	>50
20	>50	>50	>50	>50	>50	>50	>50	>50	>50
25	>50	>50	>50	>50	>50	>50	>50	>50	>50
30	>50	>50	>50	>50	>50	>50	>50	>50	>50

Table 2: Miss Distance at a Rocket-to-Target Displacement of 5000 m

$\Delta\psi \setminus \Delta\theta$ (degrees)	-10	-5	0	5	10	15	20	25	30
-30	>50	>50	>50	>50	>50	>50	>50	>50	>50
-25	>50	>50	>50	>50	>50	>50	>50	>50	>50
-20	>50	>50	>50	>50	>50	>50	>50	>50	>50
-15	>50	>50	>50	>50	>50	>50	>50	>50	>50

$\Delta\psi \setminus \Delta\theta$ (degrees)	-10	-5	0	5	10	15	20	25	30
-10	>50	>50	0.0710	0.0495	>50	>50	>50	>50	>50
-5	>50	0.0819	0.0693	0.0525	0.0405	>50	>50	>50	>50
0	>50	0.0984	0.0697	0.0530	0.0401	0.0314	>50	>50	>50
5	>50	0.0995	0.0702	0.0524	0.0393	0.0292	>50	>50	>50
10	>50	>50	38.9640	11.4701	26.6625	7.6116	>50	>50	>50
15	>50	>50	>50	>50	>50	>50	>50	>50	>50
20	>50	>50	>50	>50	>50	>50	>50	>50	>50
25	>50	>50	>50	>50	>50	>50	>50	>50	>50
30	>50	>50	>50	>50	>50	>50	>50	>50	>50

Table 3: Miss Distance at a Rocket-to-Target Displacement of 6000 m

$\Delta\psi \setminus \Delta\theta$ (degrees)	-10	-5	0	5	10	15	20	25	30
-30	>50	>50	>50	>50	>50	>50	>50	>50	>50
-25	>50	>50	>50	>50	>50	>50	>50	>50	>50
-20	>50	>50	>50	>50	>50	>50	>50	>50	>50
-15	>50	31.3999	0.0586	0.0536	0.0268	>50	>50	>50	>50
-10	>50	0.0676	0.0630	0.0442	0.0328	0.0268	>50	>50	>50
-5	0.0892	0.0894	0.0641	0.0453	0.0321	0.0240	0.0189	>50	>50
0	0.1014	0.0920	0.0639	0.0451	0.0320	0.0234	0.0181	23.2397	>50
5	0.0953	0.1176	0.0693	0.0440	0.0320	0.0231	0.0175	39.1378	>50
10	0.1203	0.0978	0.0629	0.0480	0.0356	0.0251	0.0197	>50	>50
15	>50	>50	47.2664	10.6291	22.3619	>50	12.6340	>50	>50
20	>50	>50	>50	>50	>50	>50	>50	>50	>50
25	>50	>50	>50	>50	>50	>50	>50	>50	>50
30	>50	>50	>50	>50	>50	>50	>50	>50	>50

Table 4: Miss Distance at a Rocket-to-Target Displacement of 7000 m

$\Delta\psi \setminus \Delta\theta$ (degrees)	-10	-5	0	5	10	15	20	25	30
-30	>50	>50	>50	>50	>50	>50	>50	>50	>50
-25	>50	>50	11.8709	0.0995	6.1333	>50	30.9069	>50	>50
-20	>50	0.2374	0.0447	0.0024	0.0369	0.0136	0.0647	>50	>50
-15	>50	0.1389	0.1123	0.0208	0.0269	0.0154	0.0604	0.4769	>50

$\Delta\psi \setminus \Delta\theta$ (degrees)	-10	-5	0	5	10	15	20	25	30
-10	12.5639	0.0237	0.0147	0.0351	0.0221	0.0073	0.0011	0.0004	0.0326
-5	0.3295	0.1313	0.0510	0.0273	0.0201	0.0138	0.0064	0.0103	0.0139
0	0.0533	0.1190	0.0403	0.0434	0.0255	0.0189	0.0100	0.0034	0.0305
5	0.0503	0.0510	0.0934	0.0474	0.0127	0.0172	0.0075	0.0019	0.0030
10	0.1125	0.0984	0.1159	0.0398	0.0508	0.0182	0.0100	0.0031	0.0028
15	8.0260	0.0964	0.0295	0.0465	0.0484	0.9998	2.8431	0.0300	0.0075
20	>50	>50	>50	>50	>50	>50	>50	>50	>50
25	19.8699	>50	>50	>50	>50	>50	>50	>50	>50
30	>50	>50	>50	>50	>50	>50	>50	>50	>50

Table 5: Miss Distance at a Rocket-to-Target Displacement of 8000 m

$\Delta\psi \setminus \Delta\theta$ (degrees)	-10	-5	0	5	10	15	20	25	30
-30	1.4519	1.1580	0.1321	0.1135	0.0362	0.0153	0.0145	>50	9.4038
-25	37.6822	0.1057	0.1329	0.0911	0.0144	0.0185	0.0406	>50	0.0597
-20	4.5836	0.0420	0.1835	0.1066	0.0235	0.0248	0.0141	3.8366	0.0129
-15	38.9477	0.2017	0.0474	0.0216	0.0229	0.0089	0.0006	0.0097	0.0089
-10	0.2347	0.1971	0.0819	0.0573	0.0998	0.0219	0.0343	0.0365	0.0054
-5	0.2138	0.0338	0.1435	0.0055	0.0265	0.0167	0.0177	0.0097	0.0008
0	0.1945	0.1513	0.1470	0.0149	0.0480	0.0116	0.0306	0.0081	0.0077
5	0.1719	0.2593	0.0226	0.0441	0.0468	0.0529	0.0312	0.0023	0.0078
10	0.1601	0.1946	0.1457	0.0987	0.0161	0.0074	0.0043	0.0091	0.0088
15	0.0651	0.1653	0.1731	0.0299	0.0485	0.0295	0.0303	0.0458	0.0125
20	11.6123	6.2178	7.1200	2.8860	0.1120	0.0197	4.3812	3.8366	4.8891
25	>50	>50	>50	>50	>50	>50	>50	>50	>50
30	>50	>50	>50	>50	>50	>50	>50	>50	>50

Table 6: Miss Distance at a Rocket-to-Target Displacement of 9000 m

$\Delta\psi \setminus \Delta\theta$ (degrees)	-10	-5	0	5	10	15	20	25	30
-30	25.4865	16.9399	0.2060	0.0602	0.0792	0.0666	0.0149	0.0218	0.2532
-25	0.2300	0.2121	0.1338	0.0941	0.1282	0.0315	0.0016	0.0443	0.0071
-20	0.1945	0.2274	0.1301	0.0227	0.0779	0.0503	0.0256	0.0377	0.0242
-15	0.2120	0.2196	0.0968	0.1201	0.1022	0.0072	0.0050	0.0123	0.0191

$\Delta\psi \setminus \Delta\theta$ (degrees)	-10	-5	0	5	10	15	20	25	30
-10	0.2473	0.1507	0.2034	0.1057	0.0914	0.1009	0.0125	0.0093	0.0146
-5	0.1184	0.2251	0.0870	0.1518	0.0495	0.0816	0.0151	0.0093	0.0133
0	0.2767	0.2540	0.1484	0.1271	0.0444	0.0505	0.0259	0.0118	0.0111
5	0.2846	0.0737	0.1454	0.1086	0.1338	0.0521	0.0240	0.0085	0.0150
10	0.2477	0.1067	0.0029	0.1792	0.0258	0.0546	0.0504	0.0134	0.0165
15	0.2985	0.0380	0.1577	0.0281	0.1266	0.0223	0.0304	0.0059	0.0139
20	0.3003	0.0609	4.1036	0.1523	0.0911	0.1378	0.0373	0.0024	0.0130
25	7.2814	8.0398	4.6013	11.0329	9.7683	7.5389	1.4498	6.6340	7.8275
30	>50	47.2622	4.1810	0.8245	>50	45.1004	41.6817	9.1338	10.2938

From the simulation results presented in Tables 1-6, the rocket demonstrates high accuracy, with the minimum miss distances recorded as 0.0676, 0.0292, 0.0175, 0.0004, 0.0006, and 0.0016 meters for target displacements of 4, 5, 6, 7, 8, and 9 km, respectively. Furthermore, as the displacement increases from 4 to 9 km, the rocket maintains good accuracy even when launched with a larger LOS error. This is because the reaction thruster's thrust is structurally limited, restricting the rocket's ability to change direction rapidly over time. As a result, at shorter displacement distances, the rocket has a limited turning capability. However, the results in Tables 1-6 only consider a maximum displacement of 9 km. If the displacement increases beyond this range, accuracy may degrade due to the thrust limitations of the rocket.

In this study, a Monte Carlo simulation was conducted, incorporating disturbances from atmospheric conditions and signals from the Inertial Navigation System (INS). A total of 100 simulations were performed to determine the 50% Circular Error Probable (CEP) of the rocket. The 50% CEP is defined as the radius of a circle, centered at the c.g. of target point, within which 50% of the simulated impacts are contained. The use of Monte Carlo simulations with the 50% CEP method is widely adopted and effective for evaluating the accuracy of guidance systems, particularly when assessing the uncertainties that influence the outcome of a launch.

The launch conditions followed the specifications described in Section 3.1, assuming a displacement of 6 km between the rocket and the target. The launch angles were set with $\Delta\psi = 0^{\circ}$ and $\Delta\theta = 5^{\circ}$. From the simulation results, the 50% CEP was found to be 0.0448 m, demonstrating the accuracy and reliability of the rocket's trajectory control. The analysis of the 50% CEP is illustrated in Fig. 8.

However, the analysis of the 50% CEP in this case is based on a single launch condition to demonstrate that even when the system is subjected to disturbances, the rocket can still be controlled to accurately impact the target. For other launch conditions, the 50% CEP values will vary, but the miss distances will show a similar clustering pattern as in the example case.

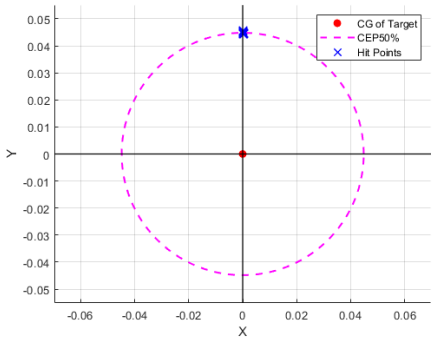

Fig 8 Analysis of the 50% Circular Error Probable (CEP)

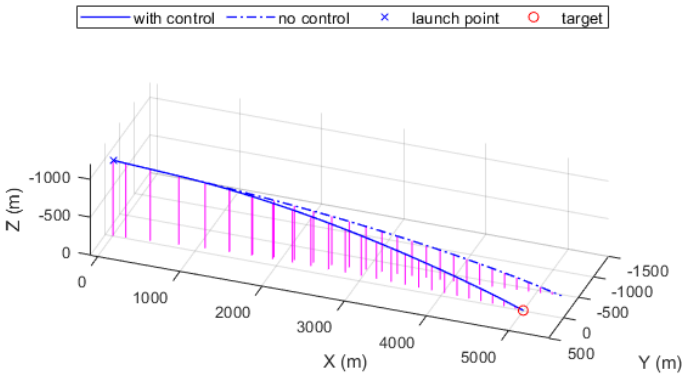

(a) 3D trajectory of the rocket

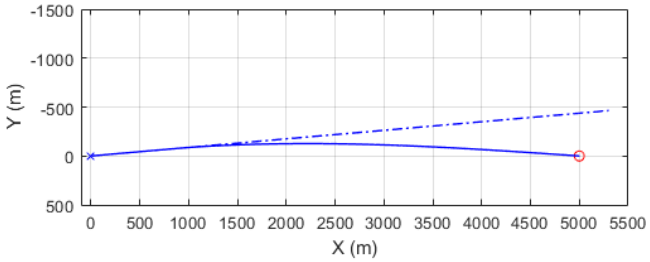

(b) Trajectory projection on the XY plane

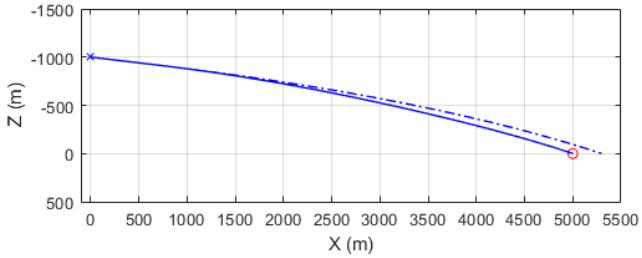

(c) Trajectory projection on the XZ plane

Fig 9 Shows an example of the trajectory from the simulation of a launch, assuming an angle of $\Delta\psi = -5^{\circ}$ and $\Delta\theta = 5^{\circ}$, with a distance of 5 km between the rocket and the target. The resulting miss distance is 0.0525 m

4. Conclusion

This paper presents a method for controlling the direction of the 2.75-inch WAFAR using a combination of pole placement and PI control to regulate the thrust output of the reaction thruster output in the guidance section. The research results demonstrate that the direction of the rocket can be accurately controlled to reach the target, and it performs well even when subjected to disturbances from the environment and noise from the system itself. This highlights the reliability of the simulation results, which were conducted using a 6-DOF model and tested with the rocket's nonlinear dynamics equations. Although the control system generates signals that are not perfectly smooth, it does not cause the rocket to lose stability during flight and provides a fast response, resulting in higher accuracy. The proposed control method is straightforward and practical for real-world applications due to its simple calculations, which do not impose a heavy processing load on the controller.

Overall, the PI control combined with pole placement can effectively be used to control the direction of the rocket under normal operating conditions. However, this approach may lack flexibility compared to more modern control techniques, especially when the rocket dynamics change significantly, which can lead to a noticeable drop in accuracy. For this study, which focuses on a 2.75-inch rocket that wasn't originally designed for guided flight, the proposed control method is sufficient to improve flight accuracy under typical usage scenarios.

However, when implementing the actual control system, the limitations of the various components, particularly the reaction thruster in terms of both structure and specific dynamics of the reaction thrust, should be carefully considered.

5. References

[1] BAE Systems, "*Advanced precision kill weapon system (APKWS).*"[Online]. Available: https://www.baesystems.com (Accessed: August. 1, 2023).

[2] M. C. Mickle, and J. J. Zhu, "Skid to turn control of the APKWS missile using trajectory linearization technique," in *Proceedings of the American Control Conference*, 2001, pp.3346-3351.

[3] W. M. Wonnacott, "*Modeling in the design and analysis of a hit-to-kill rocket guidance kit,*" M.S. thesis, Naval Postgraduate School, Monterey, CA, USA, 1997.

[4] P. H. Zipfel, "CADAC: Multi-use architecture for constructive aerospace simulations," *Journal of Defense Modeling and Simulation: Applications, Methodology, Technology,* vol. 9, no. 2, pp. 129-145, April 2012.

[5] P. H. Zipfel, *Modeling and Simulation of Aerospace Vehicle Dynamics*, 2nd ed. Reston, VA, USA: AIAA, 2007.

[6] M. Wang, G. Li, L. Zhao, and L. Wei, “Roll controller design for miniature air-to-ground missile based on ADRC,” in *2021 40th Chinese Control Conference (CCC)*, Shanghai, China, 2021, pp. 2079–2084.

[7] J. Zhou, W. Li, Q. Xia, and H. Jiang, “Robust missile autopilot design based on dynamic surface control,” *Journal of Systems Engineering and Electronics*, vol. 34, no. 1, pp. 160–171, February 2023.

[8] P. V. Rao, V. Murthy Arikapalli, S. Bhowmick, and R. Ayyagari, “Missile longitudinal dynamics control design using pole placement and LQR methods,” *Defence Science Journal*, vol. 71, no. 4, pp. 477-485, September 2021.

[9] J. Liu, K. Guo, J. Zhu, H. Wang, and J. Li, "Static unstable missiles: Design and simulation using an acceleration feedback autopilot structure," in *43rd Chinese Control Conference (CCC)*, Kunming, China, 2024, pp. 3721-3728.

[10] R. Bhattacharjee and S. Mukherjee, "Performance analysis of a missile guidance and control system model for precise target tracking," in *IEEE 3rd World Conference on Applied Intelligence and Computing (AIC)*, Gwalior, India, 2024, pp. 1471-1476.

[11] M. Zhou, D. Mao, M. Zhang, L. Guo, and M. Gong, "A hybrid control with PID–improved sliding mode for flat-top of missile electromechanical actuator systems," *Sensors*, vol. 18, no. 12, December 2018.

[12] K. Yang, "A novel PID tuning method for the missile overload control," in *2nd International Conference on Computer, Control and Robotics (ICCCR)*, Shanghai, China, 2022, pp. 86-89.

[13] D. Zhe, C. Jiabin, S. Chunlei, and C. Hongye, "Design of longitudinal control system for target missiles based on fuzzy adaptive PID control," in *29th Chinese Control and Decision Conference (CCDC)*, Chongqing, China, 2017, pp. 398-402.